International Journal of
Turbomachinery
Propulsion and Power

MDPI

Article

Improving Pressure Buildup and Water Purity in a PTJ Separation Pump †

Jessica Dafis [1,*], Xuemei Zhang [2], Katharina Zähringer [1] and Dominique Thévenin [1]

[1] Laboratory of Fluid Dynamics and Technical Flows, Otto von Guericke University Magdeburg, Universitätsplatz 2, 39106 Magdeburg, Germany
[2] State Key Laboratory of Multiphase Flow in Power Engineering, Xi'an Jiaotong University, Xi'an 710049, China; xjzxmei@stu.xjtu.edu.cn
* Correspondence: jessica.dafis@ovgu.de
† This manuscript is an extended version of the CMFF'25 paper published in the Proceedings of the International Conference on Fluid Flow Technologies, Budapest, Hungary, 26–29 August 2025.

Abstract

A modified Pitot-tube jet (PTJ) separation pump combines centrifugal phase separation with pressure buildup and enables compact oil–water treatment, where a water-rich stream can be discharged at elevated pressure. This work advances an existing laboratory PTJ configuration toward a turbomachinery-oriented rotor concept for systematic design studies and subsequent field-oriented prototypes. Starting from a centrifuge-like reference configuration without blades that prioritizes separation stability, an impeller with trimmed blades is introduced to increase pressure head while limiting blade interaction with the oil–water interface by operating primarily in the outer, water-rich annulus. Comparative experiments with and without the impeller show a pronounced increase in pressure head, up to about a factor of three at the maximum speed investigated. The results also indicate a purity penalty caused by blade-induced mixing and secondary flows. This exposes the central design trade-off of the PTJ machine. Higher specific work input increases pressure head but can reduce discharge quality. Hydraulic optimization, therefore, needs to be coupled to ppm-level purity constraints. Density-based monitoring lacks resolution in the relevant trace range, and chemical-based analyses are too slow for systematic investigations. An imaging-based fluorescence method using Nile Red as a selective tracer is, therefore, implemented as a rapid analysis tool. High-resolution imaging with automated region of interest evaluation provides a robust calibration from 5–500 ppm for safe, non-fluorescent model oils such as sunflower oil. This enables efficient operating-window mapping and comparative screening of rotor concepts under reproducible conditions.

Keywords: Pitot-tube jet separation pump; two-phase turbomachinery; trimmed blades; oil–water separation; ppm-range water quality monitoring

Check for updates

Academic Editors: János Gábor Vad, Csaba Horváth and Esztella Éva Balla

Received: 18 November 2025
Revised: 9 February 2026
Accepted: 20 February 2026
Published: 14 May 2026

Copyright: © 2026 by the authors. Published by MDPI on behalf of the EUROTURBO. Licensee MDPI, Basel, Switzerland. This article is an open access article distributed under the terms and conditions of the Creative Commons Attribution (CC BY-NC-ND) license.

1. Motivation and Environmental Context

Water pollution, especially from oil contamination, remains a major challenge for society. With increasing pressure on drinking-water resources and a rising frequency of environmental disasters, effective on-site treatment and separation solutions are becoming more important [1].

Although the Deepwater Horizon accident in 2010, which released about 800 million liters of crude oil into the Gulf of Mexico, is the best-known case, oil pollution also occurs in many everyday scenarios [2,3]. Industrial processes, shipping and the uncontrolled

discharge of bilge water at ports or through accidents at sea contribute significantly to oil contamination [4]. This issue is not limited to oceans. Inland waters such as lakes, rivers and groundwater can also be affected. Heavy rain events, floods and high tides can damage houses, vehicles and machinery containing oils, fuels and other pollutants, which can lead to groundwater contamination [4,5].

Conventional measures and treatment approaches, such as barrier systems, chemical dispersants and (controlled) burning, often show limited effectiveness and can even worsen environmental impacts [6]. There is, therefore, a strong demand for compact, robust and controllable separation and treatment devices that can be used on site and operate continuously. This enables the rapid return of purified water to the environment under defined discharge criteria. A widely used reference is a limit of 15 ppm oil in water, which is related to the MARPOL convention for bilge-water discharge [7,8].

Current treatment concepts for oil-contaminated water usually combine several stages to achieve the required discharge quality. Mechanical separation is a common basic process due to its robustness and scalability. Gravity-based separators (e.g., API separators and parallel plate separators) rely on the flotation of droplets and are suitable as pre-stages for rough dispersions. However, their separation time and space requirements increase significantly with small droplets, low density differences and disturbed operating conditions, which makes compact on-site use difficult [9–11].

High-speed centrifuges intensify the separation process and can achieve low residual oil content even with finer droplets, but they require high speeds and, therefore, involve higher investment costs, mechanical complexity and operating costs [12,13].

In accident scenarios and local oil spills, where large quantities must be handled quickly and with limited infrastructure, these compromises motivate the use of compact, on-site separation systems that combine continuous operation with low complexity and low costs while still delivering a controllable result in terms of water quality. In this study, we present an experimental investigation of a PTJ separation pump concept and its progressive development into a turbomachinery-driven head increase. First, a blade-free reference configuration is characterized to determine stable separation behavior and a feasible operating window. Next, an impeller with trimmed blades that operates mainly in the water phase is evaluated to quantify the compromise between delivery head and purity. Third, a fluorescence-based measurement method in the ppm range is introduced to support rapid operating point characterization and comparative testing under reproducible conditions.

2. PTJ Separation Pump Concept

As a possible on-site solution for oil–water treatment, earlier work at the Laboratory of Fluid Dynamics and Technical Flows at the Otto-von-Guericke University Magdeburg investigated the possibility of a compact separation system based on the hydraulic principle of a conventional Pitot pump [14–17].

In a Pitot pump, pressure is built up by using a stationary Pitot-tube to extract fluid from a rotating flow field. The concept is named after the French engineer Henri Pitot. Inside the rotating rotor, the fluid is accelerated in the peripheral direction and thus reaches its highest tangential velocity near the rotor wall [15]. The Pitot-tube extends radially from the axis of rotation into this high-velocity area and picks up the fluid. At the pick-up opening, the flow approaches a stagnation condition, so that the local dynamic pressure is largely converted into static pressure. Further downstream, the internal flow channel within the pick-up tube features a gradual cross-sectional expansion intended to reduce the mean velocity and support additional pressure recovery. In its conventional form, the Pitot pump has a single inlet and a single outlet [14].

Building on the conventional Pitot pump principle, earlier numerical studies investigated how the Pitot-tube assembly could be optimized and modified so that the concept could be used within the rotor for combined pumping and separation of a non-miscible two-phase mixture, such as an oil–water (o/w) system [16,17].

These studies showed that the Pitot-tube can be modified by adding two internal channels. When the oil–water mixture is fed into the rotor via the inlet channel, centrifugal forces induce radial phase separation. The phase separation itself occurs in the rotating rotor cavity. The phase extraction takes place at radially different positions in the rotor, allowing the water-rich outer layer and the oil-rich inner core to be continuously discharged via two separate outlets. The Pitot-tube can now perform two tasks simultaneously. It continues to extract high-speed fluid from the rotating field and convert kinetic energy into static pressure, but it can also serve as a feed and extraction element for oil–water mixtures. This combines pressure buildup and phase separation in a compact unit.

Figure 1 shows the modified Pitot-tube and the laboratory centrifuge used as the base configuration in this study. The Pitot-tube prototype (Figure 1a) was produced using additive manufacturing (Formlabs Form 3L, Clear Resin 4.1) to achieve high dimensional accuracy and comparatively smooth internal surfaces along the flow passages. The inlet for the oil–water mixture is shown in green. The outlets for the liquids separated in the rotor are divided into a high-pressure outlet (HPO) for the water-rich phase and a low-pressure outlet (LPO) for the oil-rich phase.

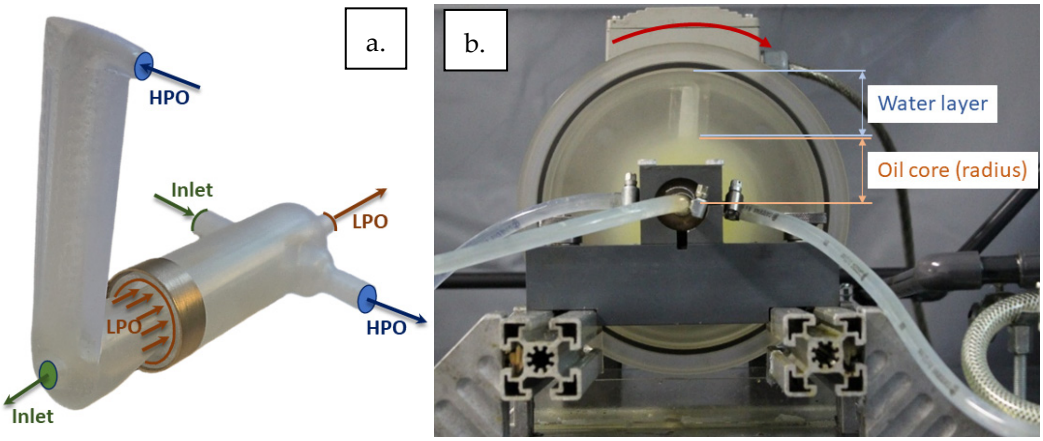


Figure 1. (**a**) Adapted Pitot-tube with one inlet and two outlets for continuous separation in a water-rich phase (HPO) and an oil-rich phase (LPO). (**b**) Front view of the laboratory PTJ test rig during operation with transparent rotor cover and a rotor inner diameter $D_{Ri} = 190$ mm. The red arrow indicates the direction of rotation.

The adapted Pitot-tube is installed in a laboratory centrifuge. Figure 1b shows the base configuration at laboratory scale, which serves as the starting point for systematic operating-point studies and for subsequent rotor and impeller development. In contrast to earlier work that focused primarily on numerical feasibility studies, the present work develops and presents an experimental test rig concept to demonstrate feasibility under controlled laboratory conditions. The rotating separator has a transparent front cover that provides visual access to the internal phase distribution and allows for quick replacement of internal geometries. Flexible hoses connect the channels within the Pitot-tube to the rest of the system. The inner diameter of the rotor is $D_{Ri} = 190$ mm, and the red arrow shows the rotation direction. In this initial state, the pump is operated without any bladed impeller.

In contrast to our earlier PTJ separation studies that focused primarily on demonstrating separation capability and establishing operating windows, the present work shifts the emphasis toward a turbomachinery-driven pressure head increase while maintaining

separation performance. The novelty lies in the rotor concept, which introduces a dedicated impeller element specifically trimmed to act mainly within the outer, water-rich annulus of the PTJ rotor, enabling controlled head gains with minimized direct blade interaction with the oil-rich core. This design is implemented in a modular laboratory platform that allows for direct back-to-back comparison of internal rotor geometries under identical boundary conditions.

3. Experimental Setup, Methods and Performance Metrics

The test facility is designed as an open system. Water and oil are drawn from separate storage tanks, and the separated phases are directed to collection tanks after the separation process. A schematic flow diagram is shown in Figure 2.

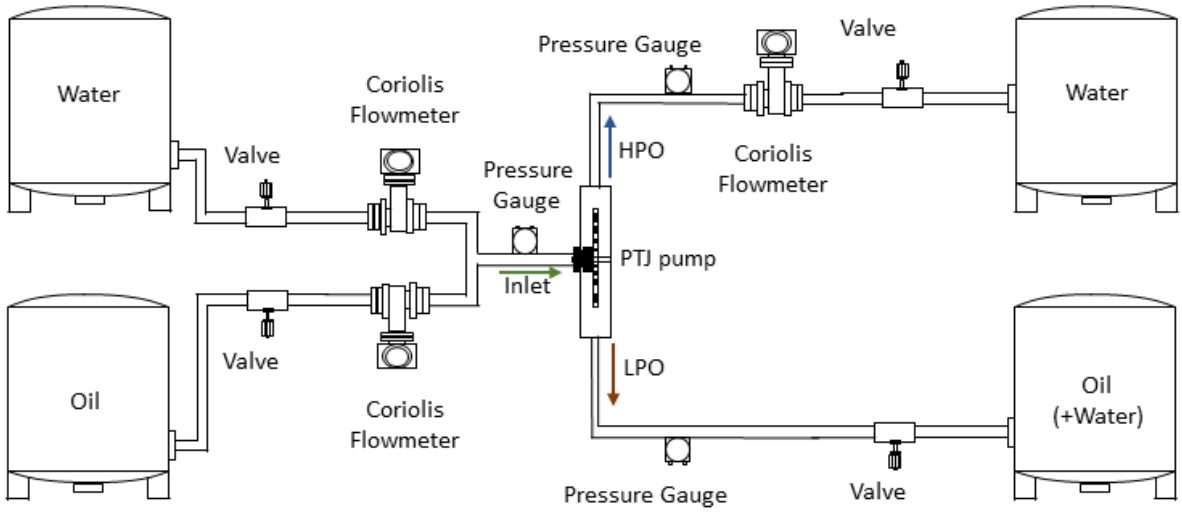


Figure 2. Experimental test setup of the PTJ pump at pilot scale. The arrows indicate the inlet path and the separate outlet paths (HPO and LPO).

The water and oil tanks supply a mixture of controlled composition to the PTJ separation pump. Both tanks are open to the atmosphere, so the free surfaces are at ambient pressure. Hoses and pipes route both phases to the centrifuge inlet at the Pitot-tube.

The volumetric or mass flow rate of each phase is adjusted using fine-control valves. A scale on each valve enables reproducible settings and documentation of the operating point during measurement campaigns.

The two outlet lines of the separation pump, the HPO for the water-rich phase and the LPO for the oil-rich phase, are connected to separate collection tanks. Submersible pumps installed in these tanks allow the fluids to be disposed of or returned to the storage tanks. This arrangement enables longer test series under nearly constant boundary conditions without consuming large amounts of test fluid.

3.1. Measurement System

To quantify the separation and pumping performance, the pressure, p; mass flow rate, $\dot{m}$; density, ρ; and temperature, T, are measured at several points in the plant, as shown in Figure 2. Coriolis flowmeters (CF; Proline Promass 83E, Endress + Hauser, Stahnsdorf, Germany) measure $\dot{m}$, ρ and T in both pure substance paths and at the HPO. The pressure is measured with piezoresistive pressure transmitters (Cerabar T PMP131, Endress + Hauser, Stahnsdorf, Germany) at the inlet and at both outlets, with a measurement accuracy of 0.5%.

The data is acquired using measurement hardware from National Instruments (Austin, TX, USA) and recorded and evaluated using DIAdem. This enables time-resolved measurements, real-time visualization and subsequent post-processing.

3.2. Test Fluids and Material Properties

Water and sunflower oil are used as a reference system for an immiscible two-phase flow. Sunflower oil was selected as the model oil because it is non-toxic, readily available and inexpensive. It is also comparatively stable in storage, handling and disposal compared with many mineral oil products. At the same time, sunflower oil represents a conservative separation case. Its density difference to water is relatively small, its viscosity is comparatively high, and it readily forms emulsions. Successful separation of sunflower oil–water mixtures, therefore, suggests that lighter mineral oils with larger density differences can generally be separated more easily under otherwise comparable conditions.

Table 1 summarizes the densities of selected fluids at 20 °C. It includes water and sunflower oil; other vegetable oils; and technical media such as engine oil, diesel fuel and heating oil.

Table 1. Densities of different fluids already tested in the laboratory test rig [18–21].

	Density at ~20 °C [kg/m^3]
Water	998
Sunflower Oil	918–923
Olive Oil	910
Rapeseed Oil	907
Engine Oil	855–907
Gasoline	720–767
Diesel fuel	802–886
Heating Oil	815

The density difference to the water phase is a key driver of centrifugal separation. A larger density difference generally increases the characteristic Stokes terminal velocity:

$$v_{term} = \frac{(\rho_d - \rho_c)\, g \cdot d_d^2}{18 \cdot \mu}. \quad (1)$$

Here, ρ_d is the density of the dispersed phase (oil droplets), ρ_c is the density of the continuous phase (water), d_d is the droplet diameter, μ is the dynamic viscosity of the continuous phase, and g is the gravitational acceleration.

For otherwise identical conditions, the Stokes terminal velocity, v_{term}, scales linearly with the density difference, $\Delta\rho$, between oil and water. For droplet sizes of about 100 µm, a sunflower oil–water system with $\Delta\rho \approx 81$ kg/m^3 results in a Stokes terminal velocity of $v_{term} \approx 0.7$ mm/s. For a mixture with diesel fuel, $\Delta\rho \approx 167$ kg/m^3 results in $v_{term} \approx 1.4$ mm/s. The diesel fuel–water system, therefore, exhibits more than twice as high a Stokes velocity in this simplified estimate. Although separation in the PTJ rotor is dominated by centrifugal forces, this simplified estimate illustrates the importance of density difference in separation behavior.

3.3. Operating Point Parameters and Objectives

Two key objectives are evaluated within the experimental setup: (i) the oil fraction at the high-pressure outlet, α_{HPO}, and (ii) the pressure head, H_{HPO}. This supports the identification of relevant operational parameter ranges and system optimization.

The oil fraction at the HPO is calculated from the measured densities at the inlet path and at the HPO:

$$\alpha_{HPO} = \frac{\rho_{HPO} - \rho_{Water}}{\rho_{Oil} - \rho_{Water}}. \quad (2)$$

Here, ρ_{HPO} is the density measured at the HPO; ρ_{Oil} and ρ_{Water} are the densities of the pure phases at the measured temperature.

The pressure difference, Δp, is converted into a pressure head using Equation (3). This represents the height the pump can overcome in a field scenario, for example, due to elevation changes or hydraulic losses:

$$H_{HPO} = \frac{\Delta p}{\rho_{HPO} \cdot g}, \quad (3)$$

with $\Delta p = p_{HPO} - p_{in}$. The pressure, p_{HPO}, is measured in the HPO line directly behind the pump, and the inlet pressure, p_{in}, is measured in the inlet path before the pump (see Figure 2, positions of the pressure gauges). Internal potential-energy differences are negligible due to the compact setup.

One operating point of the PTJ pump is defined by four variable parameters: (i) inlet oil fraction, α_{in}; (ii) rotational speed, n; (iii) inlet mass flow rate, $\dot{m}_{in}$; and (iv) flow split ratio, FS:

$$FS = \frac{\dot{m}_{LPO}}{\dot{m}_{in}} = 1 - \frac{\dot{m}_{HPO}}{\dot{m}_{in}}, \quad (4)$$

which is defined as the ratio of the mass flow rate at the LPO to the inlet mass flow rate. It is essential for controlling phase discharge and maintaining stable separation, as discussed in [17].

3.4. Results of the Baseline Configuration

A large test matrix was prepared by considering reproducible valve settings. The operating parameters α_{in}, $\dot{m}_{in}$, n and FS were varied systematically. The rotational speed, n, is set via the motor frequency inverter. The corresponding feedback signal is recorded in DIAdem, together with the sensor data. In addition to sunflower oil, heating oil, diesel, gasoline, olive oil and engine oil were tested to cover a range of density differences and interfacial behavior with water.

Figure 3 shows representative separation states for different oils at a fixed operating point. During operation, the inner oil core reaches a quasi-steady diameter if the boundary conditions remain stable. The oil-core diameter is influenced by α_{in}; the flow split, FS; and fluid properties such as viscosity, density and interfacial tension. Changes in oil-core size directly affect the risk of oil carry-over into the HPO and, therefore, constrain the achievable water purity.

At a given speed, the permissible mass flow rate is limited by the available residence time in the rotor and the associated separation time in the centrifugal field. Increasing the inlet flow rate increases the flow velocities and shear near the oil–water interface, promotes droplet entrainment, and reduces the time available for radial droplet migration. This leads to a compromise between flow rate and purity: a higher flow rate can lead to water being transported into the LPO (and, in the worst-case scenario, oil being transported into the HPO) if the interface is displaced or destabilized. The observed water content in the LPO at higher flow rates is, therefore, to be expected. Conversely, for a cleaner oil extraction, it would be possible to adjust the LPO radius to reduce transport from the water-rich annular region.

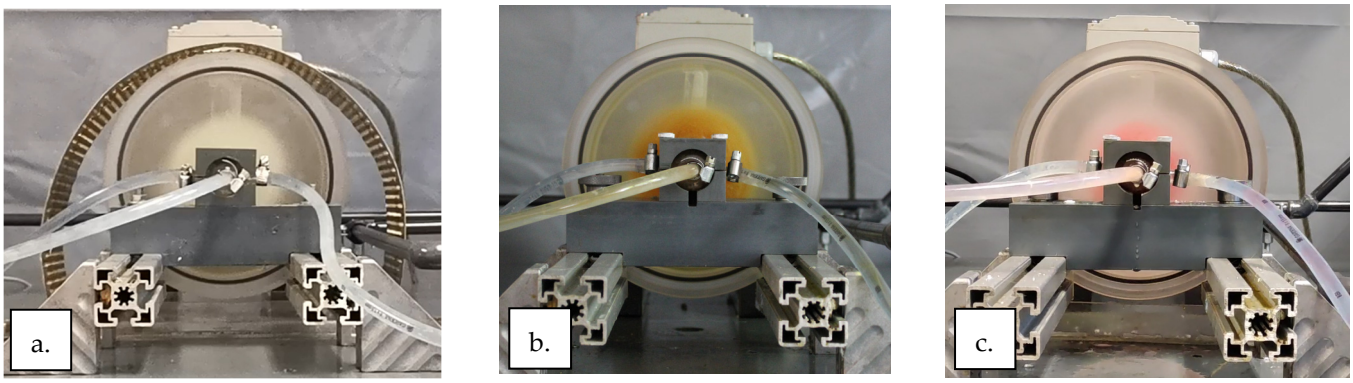


Figure 3. Representative photographs of the separation process for the operating point $\dot{m}_{in} = 160$ kg/h, $\alpha_{in} = 0.3$, n = 450 min^{-1} and FS = 0.7 using (**a**) sunflower oil, (**b**) engine oil and (**c**) heating oil.

According to Equation (2), density-based evaluation reliably distinguishes between operating states with strong and weak separation. For each steady operating point, $N = 150$ values are recorded for each density signal. The empirical standard deviation is $\sigma_\rho \approx 0.33$ kg/m^3. Using linear uncertainty propagation for a typical sunflower oil–water system with $\Delta\rho = 78.3 \ldots 86.4$ kg/m^3 and a 95% confidence interval, the resulting uncertainty of the density-based oil fraction is $\pm 1.08 \ldots \pm 1.19$ vol.%. Density measurements are, therefore, valuable for rapid monitoring and for detecting large contaminant proportions, but they cannot resolve the low ppm range required to assess the 15 ppm discharge target mentioned in the introduction.

To better quantify residual oil content, selected HPO water samples were analyzed externally by total organic carbon (TOC) analysis. Depending on the operating conditions, almost all TOC results indicated residual oil below 80 ppm, many operating points were around 5 ppm, and the best cases were around 2 ppm. These results confirm that the PTJ separation concept can achieve high water purity when operated within a defined parameter window that ensures stable separation. The experiments also showed that fuels and many technical oils, such as diesel, heating oil and engine oil, can be separated effectively. This supports the relevance of the concept for the treatment of oil-contaminated water. The measurement limitations above also show that dedicated methods are required for the evaluation of the residual oil content in the ppm range during optimization.

In this first development phase, the focus was on water purity. The rotor was, therefore, operated without an impeller to minimize shear-induced remixing and to quantify the separation behavior. In this configuration, the pressure head depends primarily on rotational speed, n. Figure 4 shows the pump characteristics of the laboratory PTJ system at $n = 300$ min^{-1}; 450 min^{-1}; 600 min^{-1}; and 750 min^{-1}. The symbols represent measured operating points, and solid curves show quadratic trend-line fits to visualize the centrifugal-pump-like behavior. As the total flow rate, Q, increases, the pressure head, H_{HPO}, decreases slightly with an approximately parabolic shape.

The dominant driver for pressure buildup is the rotational speed. Increasing n shifts the characteristic curve to higher pressure heads. This is consistent with similarity laws with an approximately quadratic scaling of pressure head with speed. Variations in α_{in}, $\dot{m}_{in}$ and FS do not lead to a significant change in H_{HPO} within the investigated range.

Although higher rotational speeds improve hydraulic performance, the usable speed is limited by separation stability. Above about $n = 900$ min^{-1}, partial remixing occurs.

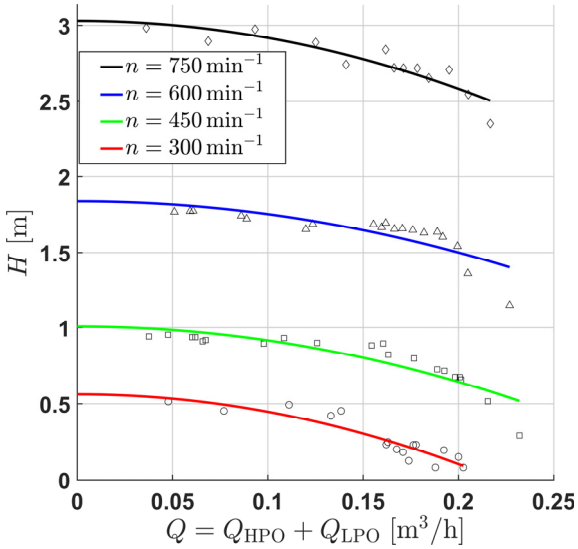


Figure 4. Pump characteristic curves of the PTJ separation pump with the pressure head, H_{HPO}, relative to the total flow rate, Q, at increasing rotational speeds, n. Symbols indicate measured operating points, and solid lines show quadratic least-squares trend lines.

An important reason for this is the increasing turbulence around the stationary Pitot tube. Based on the local circumferential velocity at the pickup radius, $r \approx 93$ mm, and the characteristic length of the Pitot head (chord $c \approx 27.9$ mm), the Reynolds number, Re, is on the order of Re $\approx 1.2 \times 10^5$ at $n = 450$ min^{-1} and increases proportionally with n (for example, Re $\approx 2.4 \times 10^5$ at $n = 900$ min^{-1}). This causes the flow to become increasingly turbulent. At very high n values, turbulence and shear generated by the stationary pick-up tube promote emulsification. The oil core becomes destabilized, and residual oil in the HPO stream rises. This becomes unacceptable when keeping in mind the central objective of minimizing α_{HPO} and achieving ppm-level purity.

Once a suitable operating range for stable separation has been identified, increasing the pressure head solely by further increasing the speed is, therefore, not possible. A turbomachinery-based approach is required to increase pressure buildup while limiting additional shear at the oil–water interface. This motivated the development of a modified rotor concept with an impeller or blade geometry designed to act primarily in the outer, water-rich annulus.

To support subsequent development steps, a first operating window was derived from the experimental dataset. A correlation-based screening confirmed that the operating parameters affect the pressure head and residual oil content in different ways. The screening quantifies the strength of these effects, but it does not, on its own, define acceptable operating conditions. In addition, the density-based oil fraction derived from Coriolis measurements has a practical uncertainty of $\pm 1.08 \ldots \pm 1.19$ vol.%, as explained previously. For this reason, operating points were preferred, where the density-based HPO oil fraction remained below $\alpha_{HPO} \leq 0.01$, corresponding to the measurement uncertainty. The resulting parameter ranges define a favorable operating window for the PTJ separation pump:

i. $n \approx 300$ min^{-1} to 750 min^{-1};
ii. α_{in} up to 0.45;
iii. $\dot{m}_{in} \approx 61.2$ kg/h to 237 kg/h (keep in mind the small size of the prototype);
iv. $FS \approx 0.69$ to 0.91.

These ranges are suitable for systematic test rig investigations of separation and pressure head performance. They provide a robust starting point for operating-point sweeps and for back-to-back comparison of modified rotor concepts.

4. Impeller Design and Implementation

This section describes and evaluates an impeller-equipped rotor concept that shifts the developed device towards turbomachinery-like operation. A dedicated impeller was developed for the PTJ configuration to increase pressure head while maintaining separation purity. To limit shear at the oil–water interface, the impeller is designed to operate only in the outer, water-rich annulus. By restricting blade action to this region, interaction with the oil core is reduced, which limits remixing and enables a higher pressure head for the water-containing outlet. This supports operation within the previously identified window that provides stable phase separation.

The impeller presented here is a modular proof of concept to increase the pressure head of the water-rich discharge while maintaining separation stability. It must be kept in mind that the flow environment differs from that of a conventional centrifugal pump. The rotor cavity exhibits strong pre-swirl due to the rotating flow field, whereas the imposed throughflow is comparatively small. Consequently, the meridional (radial) velocity component is much smaller than the circumferential component, and classical inlet design assumptions and "shock-free entry" criteria of volute-type centrifugal pumps are not directly applicable.

The design objective was, therefore, not to realize an optimized centrifugal pump impeller but to introduce a simple rotating work element acting primarily in the outer, water-rich annulus and to experimentally quantify the resulting head–purity trade-off. A full-radius blade concept was used as a geometric starting point, and the central region was subsequently removed based on an oil-core diameter estimate.

The impeller was developed in two steps. First, a full-radius blade concept was defined as a reproducible geometric starting point. For this initial layout, the inner diameter was set to $D_1 = 54$ mm to match the drilling diameter required for the sealing ring and the Pitot-tube shaft passage. The outlet diameter was set to $D_2 = 190$ mm and the blade thickness to $e = 4$ mm. The blade angles β_1 and β_2 were selected as initial screening parameters for this pre-swirling rotor environment to obtain a robust proof-of-concept geometry; they are not presented as an optimum derived from conventional centrifugal-pump inlet design criteria. The blade shape was parameterized using a single-arc construction to define the CAD geometry in a reproducible manner:

$$\kappa = \frac{\left(\frac{D_2}{2}\right)^2 - \left(\frac{D_1}{2}\right)^2}{2\left(\left(\frac{D_2}{2}\right)\cos\beta_2 - \left(\frac{D_2}{2}\right)\cos\beta_1\right)}. \tag{5}$$

The parameter κ is used as a geometric descriptor of the chosen baseline blade shape, not as an optimization outcome from classical pump design correlations. Using the values $D_1 = 54$ mm, $D_2 = 190$ mm, $\beta_1 = 20°$, $\beta_2 = 30°$, this yields a curvature radius of approximately 73 mm (geometric definition of the baseline CAD).

In the second step, the impeller inlet region was trimmed so that the blades operate only in the water phase near the rotor wall. The tested trimmed configuration starts at $D_1 = 120$ mm and extends to $D_2 = 190$ mm so that the blade's leading edge remains in the outer, water-rich annulus. This requires a reliable estimate of the oil-core diameter under operation.

4.1. Estimating the Oil Core Diameter

Assuming a closed system, this calculation is relatively simple. The oil core diameter, D_{OC}, can be determined from the total rotor diameter, taking into account the volume fraction of oil inside:

$$D_{OC} = \sqrt{\alpha_{in} \cdot D_{Ri}^2 + D_{Pt}^2}. \tag{6}$$

Here, $D_{Ri}(= D_2)$ is the inner rotor diameter, D_{Pt} is the Pitot-tube shaft diameter in the centre (34 mm), and α_{in} is the oil fraction at the inlet.

Equation (6) assumes a sharp interface and no continuous extraction. Under these assumptions, minimum oil-core diameters can be estimated. Figure 5 shows the calculated cross-section for inlet oil fractions of 0.2, 0.3 and 0.4. The Pitot-tube shaft occupies the central region, and the oil core forms a cylindrical ring around it. The outer region towards the rotor wall is the water layer.

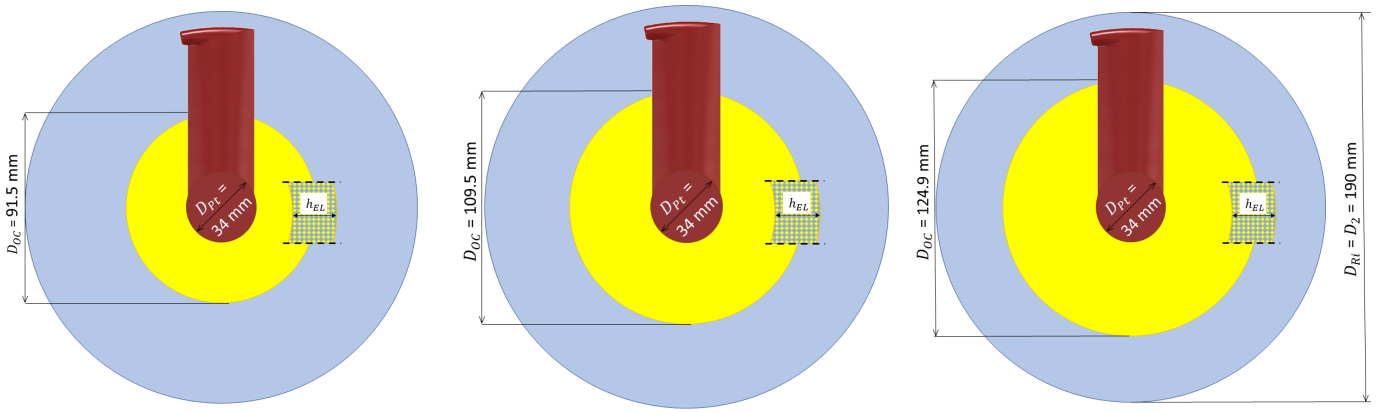


Figure 5. Calculated oil core diameters (yellow) for α_{in} = 0.2 (**left**); α_{in} = 0.3 (**middle**); and α_{in} = 0.4 (**right**), with an additional (unknown) emulsion layer thickness, h_{El}.

In reality, the interface is not perfectly sharp. The Pitot-tube induces turbulence, which can promote mixing near the interface and form an emulsion layer of unknown thickness h_{El} between the oil core and the water layer. The emulsion-layer thickness depends on operating conditions and oil properties such as density, viscosity and interfacial tension.

During continuous operation, oil-core estimation becomes more complex. The inlet oil fraction affects core size, but the flow split ratio also matters. Depending on FS, part of the water is removed via the HPO and part of the oil via the LPO, which changes the phase balance inside the rotor. A simplified estimate would assume that the HPO transports only water and the LPO only oil. In practice, the LPO typically contains a water fraction, often in the order of 10% or more. This fraction depends on oil properties and operating point, which also affect emulsion thickness and core stability.

A detailed predictive model could be formulated, but its practical value would be limited because oil properties and operating conditions vary with time and application scenario. The impeller was, therefore, designed for a representative target case. The focus was set on operating conditions that provided high separation performance, with $\alpha_{in} \approx 0.3$. Using Equation (6) with $\alpha_{in} = 0.3$, $D_{Ri} = 190$ mm, and D_{Pt} = 34 mm, the estimated oil-core diameter is D_{OC} = 109.5 mm. A safety margin of 10% was applied to account for the emulsion layer, which yields a design value of $D_{OC} \approx 120$ mm. The full-radius impeller was trimmed accordingly.

4.2. Blade Geometry and Implementation

The resulting blade geometry is shown in Figure 6. Panel (a) shows the full-radius impeller. Panel (b) shows the trimmed variant. A cylindrical cut with a diameter of 120 mm removes the central blade region. Only the outer radial blade section from D_1 = 120 mm to D_2 = 190 mm remains, so the blades rotate in the water-rich annulus.

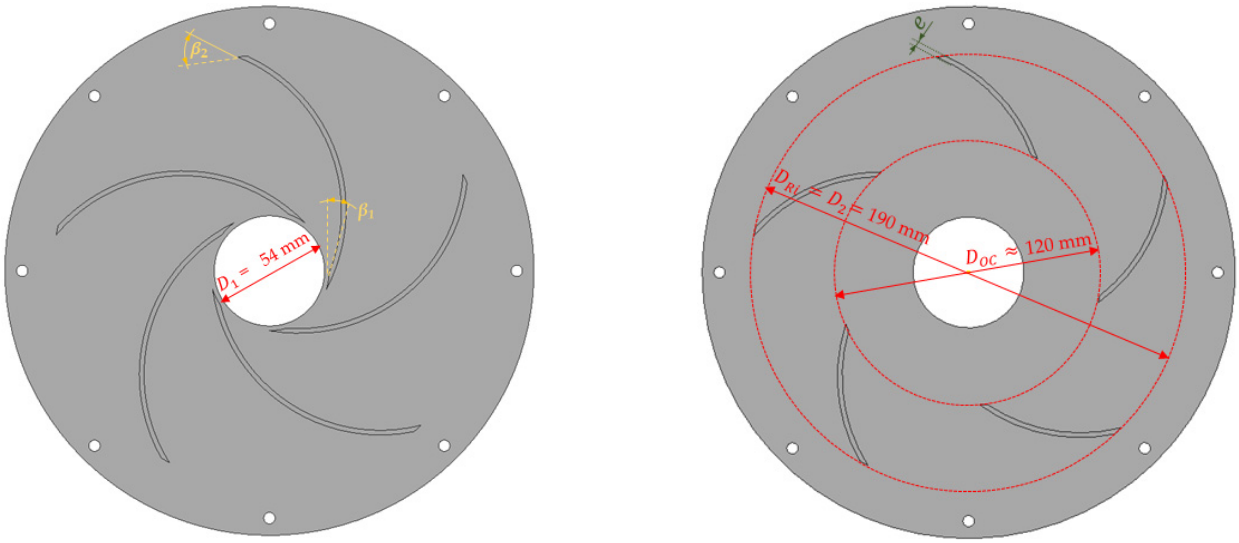


Figure 6. Front view of (**a**) full-length impeller blades and (**b**) blades cut to operate only in the outer water layer (near the periphery).

The test rig uses a modular rotor cover plate to enable rapid replacement and back-to-back comparison of internal geometries. The transparent front cover provides visual access to the phase distribution and can be exchanged quickly. The cover plate, together with the impeller and its trimmed blades (Figure 6b), was installed in place of the original cover without blades. The rotor and cover plate have an outer diameter of 230 mm. The cover plate is sealed and bolted to the rotor to ensure tightness and accurate alignment of the blades inside the rotor cavity.

4.3. Experimental Evaluation of Blade Influence

Comparative experiments were performed with two rotor configurations. The first configuration corresponds to the blade-free reference design and behaves like a centrifuge, as shown in Figure 1b. The second configuration uses a modified cover plate with shortened blades that rotate in the outer, water-rich annulus. Figure 7 shows the concept. The left image shows the impeller at standstill. The right image shows the PTJ pump in operation at a representative operating point (FS = 0.7; $\dot{m}_{in}$ = 120 kg/h; $\alpha_{\mathrm{in}} = 0.3$; $n = 450\ \mathrm{min}^{-1}$).

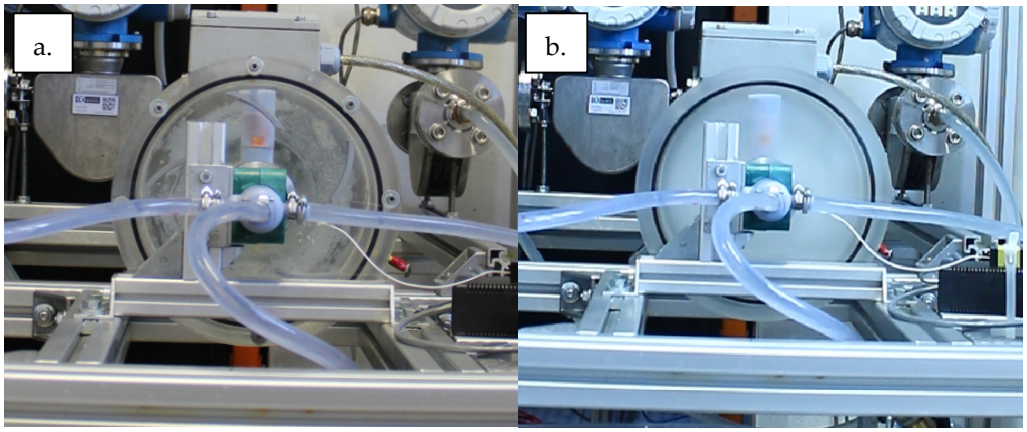


Figure 7. Impeller configuration with trimmed blades in the laboratory PTJ test rig. (**a**) Installed cover plate with shortened blades in the separator at standstill (front view through the transparent rotor cover). (**b**) PTJ pump in operation with the impeller at a representative operating point.

This operating point lies within the favorable separation range identified for the reference configuration. For the evaluation, rotational speed and inlet mass flow rate were varied systematically, and their influence on pressure head and water purity was analyzed.

As expected, adding blades increased the pressure head compared with the blade-free configuration at the same rotational speed. Figure 8 shows the H/Q characteristics at $n = 450\ \mathrm{min}^{-1}$ for both configurations. Both curves show a decreasing trend towards higher flow rates. The decline is steeper for the bladed configuration. With increasing Q, the interface became less stable with the bladed cover plate. Across the investigated speed range, the bladed configuration systematically achieved a much higher pressure head than the blade-free configuration. Future work will extend the operating range mapping for the bladed configuration. This requires a refined definition of the permissible operating window based on separation quality to ensure that the water purity targets are met.

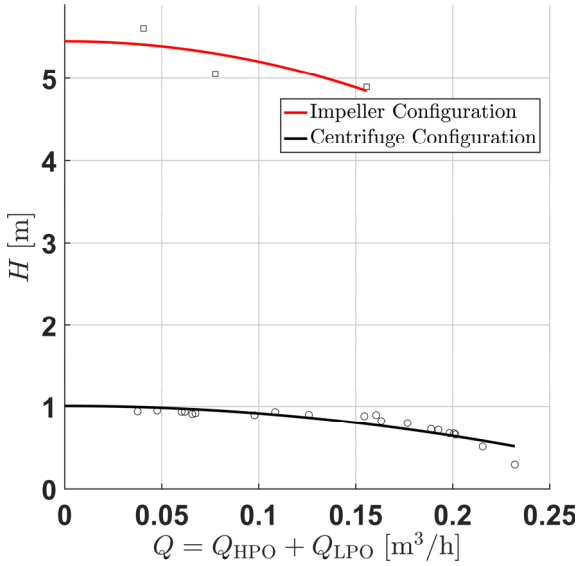


Figure 8. Pump characteristic curves at constant rotational speed $n = 450\ \mathrm{min}^{-1}$ for the centrifuge configuration (without blades) and for the impeller configuration with trimmed blades.

To quantify residual oil in the purified water stream, a water sample was taken at the HPO for each speed and rotor configuration and analyzed by TOC analysis. Residual oil concentrations at the HPO are reported as $c_{o/w}$ in ppm $\approx$ mg/L. For the blade-free configuration, all measured values were $c_{o/w} \leq 15$ ppm, with best cases down to about 2 ppm. For the bladed configuration, TOC indicated 20 ppm $\leq c_{o/w} \leq 45$ ppm. These values are technically relevant but do not meet stringent maritime discharge limits. Since only part of the operating range has been investigated so far, and operating parameters have not been optimized for minimum residual oil, the results reveal clear improvement potential. A tighter restriction of the permissible operating range and targeted adjustment of the flow split are expected to reduce $c_{o/w}$ further while maintaining the head gain provided by the impeller.

From a turbomachinery perspective, these results highlight the central design trade-off of the PTJ machine. Higher specific work input increases pressure head, but blade-induced shear and secondary flows promote interfacial entrainment and reduce water purity. Impeller development for PTJ separation pumps, therefore, requires a concurrent assessment of hydraulic performance and ppm-level purity targets at the HPO.

The present impeller is a modular proof of concept rather than an optimized final design. Its purpose is to make the head–purity trade-off measurable and to provide a reproducible baseline for comparing alternative concepts that reduce interfacial shear. Candidate

approaches include casing-side vanes, the Pitot shape acting on the water annulus, and modified blade shapes or placements that limit secondary flows near the interface.

Systematic optimization requires fast purity feedback during operating-point sweeps. This is not achievable with density-based monitoring or external laboratory analytics alone. Density-based mass balances using Coriolis meters reach a practical resolution limit well above the relevant contamination levels. External TOC analysis is sufficiently sensitive but too slow and costly for systematic tests and iterative geometry modifications. A rapid ppm-range oil-in-water detection method is, therefore, required to quantify blade-induced remixing and to map the permissible operating range for each rotor geometry directly at the test rig. This requirement motivates the fluorescence-based measurement approach briefly introduced in the next section [22].

5. Fluorescence Method for ppm-Range o/w Quantification

5.1. Experimental Setup

The next development step for the PTJ separation pump requires a laboratory method that links turbomachinery testing to discharge-relevant water quality. The goal is to evaluate rotor and impeller variants on the test rig with short iteration cycles. This includes defining a permissible operating range for each geometry and identifying settings that maintain pressure head while meeting ppm-level purity targets. To enable this workflow, an imaging-based fluorescence method was implemented as a rapid, reproducible ppm-range tool for oil-in-water quantification under controlled laboratory conditions.

Figure 9 shows the laboratory setup. The sample is filled into a cuvette and placed at a fixed position in front of a monochrome CMOS camera (FLIR Blackfly S, 5 MP, 16-bit) equipped with a 60 mm Nikon F-mount lens (NIKKOR) and a 555 nm long-pass filter. Fluorescence is excited by green LEDs that illuminate the cuvette from both sides. A black enclosure suppresses ambient light so that the recorded grayscale intensity is dominated by the fluorescence emission of the sample.

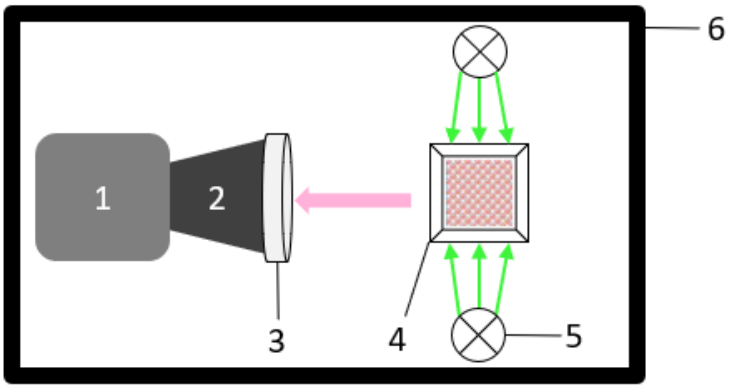


Figure 9. Schematic setup for fluorescence imaging of oil in water samples. The system consists of a CMOS camera (1), an objective lens (2), a long-pass filter (3), a cuvette filled with the prepared emulsion sample (4), LED illumination on both sides (5) and a light-shielding housing (6) (reprinted from [23]).

Figure 10 illustrates the fixed cuvette position and the automated selection of the region of interest (ROI). The ROI excludes edge regions near the cuvette walls, where refraction and reflections disturb the signal. Since the cuvette position is exactly fixed, the same ROI can be applied to all images. This improves repeatability across large measurement campaigns.

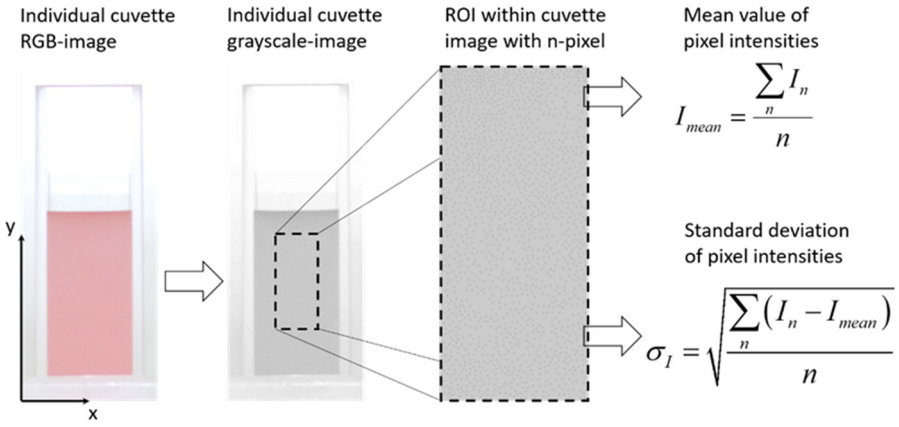


Figure 10. Example image of the cuvette and definition of the region of interest used for evaluation. The ROI is placed away from the cuvette walls to reduce optical distortion and reflections.

In this study, the workflow is tailored to PTJ operating-point investigations. All images are acquired under fixed optical settings and evaluated using an automated ROI procedure. This enables the rapid and reproducible conversion of image intensity into ppm-level concentration estimates for large parameter sweeps. It directly supports turbomachinery screening, where many rotor and operating-point combinations must be compared under consistent boundary conditions.

5.2. Tracer Concept and Spectral Verification

During laboratory development, sunflower oil is used as the standard model oil for safety and cost reasons. For sunflower oil, most commercially available oil-in-water sensors do not provide reliable results in the relevant ppm range. Therefore, the laboratory-compatible fluorescence imaging method was implemented to support PTJ optimization with rapid feedback.

Pure sunflower oil exhibits only weak fluorescence under practical excitation conditions. To obtain a stable and strong optical response, sunflower oil is dyed before use. Nile Red (NR) is added as a selective tracer to the oil phase at a defined concentration of 1 mg/L. This tracer is insoluble in water and binds only to dispersed oil droplets. This selectively labels the oil phase and improves the signal-to-noise ratio at low concentrations.

Figure 11 compares the emission spectra of pure sunflower oil and sunflower oil dyed with Nile Red at an excitation wavelength of 535 nm. This wavelength matches the green LEDs used in the setup and lies in the range where Nile Red shows a strong fluorescence response. Under these excitation and detection conditions, pure sunflower oil does not provide any fluorescence signal for quantifying oil in water in the ppm range (the small peak visible in Figure 11 corresponds to a reflection of the excitation source). In comparison, the dyed sunflower oil exhibits a pronounced emission peak in the expected spectral range of Nile Red. This provides the basis for a robust calibration curve and reproducible ppm-range measurements in the laboratory.

Using Nile Red also improves reproducibility across long measurement campaigns. Intrinsically fluorescent vegetable oils such as olive oil can show signal variations due to oil type, processing, storage and aging. This would require frequent recalibration and would reduce comparability across test series. With sunflower oil and a defined Nile Red concentration, the optical response is controlled and repeatable so that a single calibration can be reused under fixed optical settings.

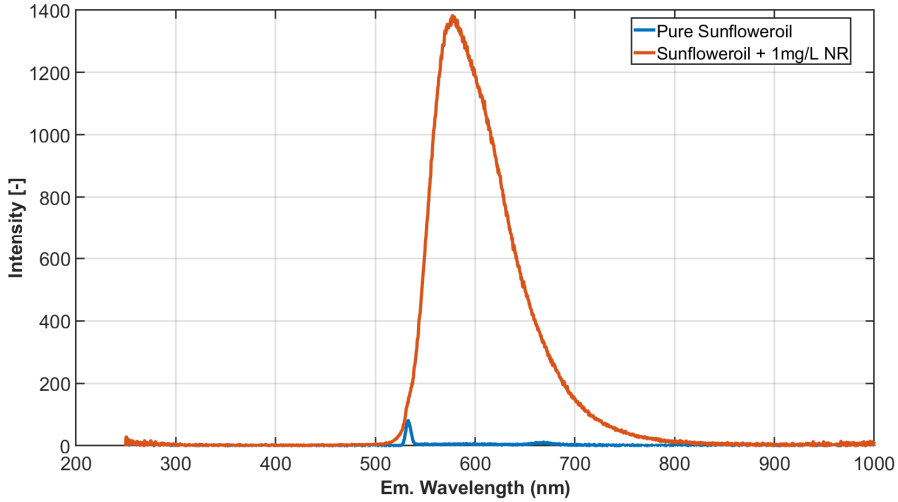


Figure 11. Emission spectra of pure sunflower oil (blue) and sunflower oil with Nile Red (orange) at a tracer concentration of 1 mg/L, recorded at an excitation wavelength of 535 nm (small peak in the blue line).

5.3. Sample Preparation and Calibration Workflow

The fluorescence-based oil-in-water methodology relies on a calibration curve and, therefore, requires a stable and reproducible emulsion. Generating a stable oil–water mixture without emulsifiers requires high-energy mixing to create fine dispersed oil droplets. A stable emulsion is essential because fluorescence imaging assumes a homogeneous droplet distribution for reliable quantification.

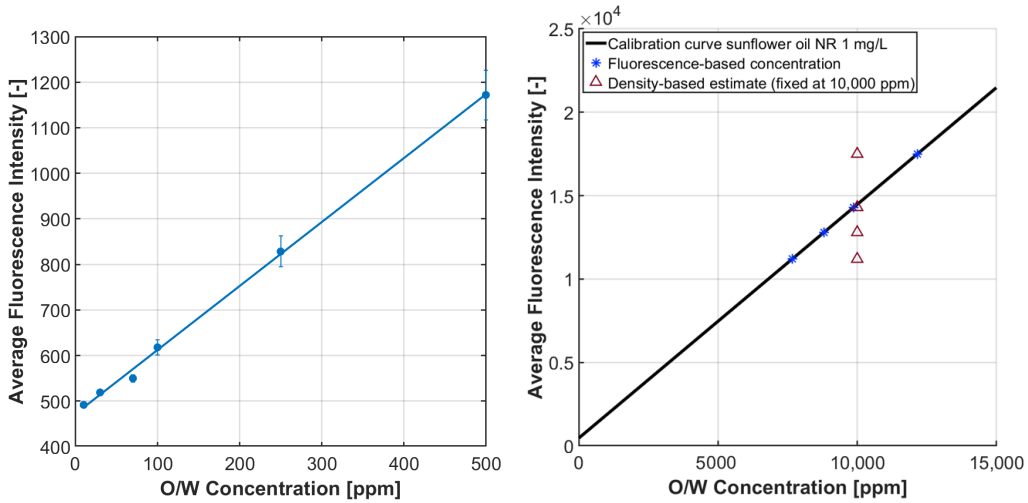
In this study, a Polytron PT3100 homogenizer was used. It handles up to a 2 L total volume and provides a maximum rotational speed of 12,000 min^{-1}. Even at this speed, the emulsion remained stable for about three minutes. Measurements were, therefore, performed quickly before phase separation begins. The preparation procedure was standardized for all experiments [24].

A volume of 200 mL of deionized water was mixed with a defined amount of dyed sunflower oil to obtain the target oil-in-water concentration. The mixture was dispersed at 12,000 min^{-1} for 120 s. After emulsification, samples were transferred into disposable cuvettes and positioned in front of the CMOS camera. All measurements were performed at a constant exposure time of 5000 µs.

All images were acquired under fixed camera settings, including exposure time and fixed illumination geometry. Grayscale values were, therefore, comparable across the dataset. For each image, the mean grayscale intensity within the predefined ROI was used as the primary signal. The ROI was kept constant to avoid wall-reflection and refraction artifacts and to maximize repeatability. The resulting mean intensity values were then correlated with the known calibration concentrations to obtain a regression equation. This equation was applied to PTJ outlet samples prepared and evaluated using the same workflow and optical settings.

5.4. Results and First PTJ Sample Check

A concentration-dependent calibration curve was established based on the setup described above. Figure 12a shows the correlation between oil-in-water concentration and mean fluorescence intensity. Each concentration corresponds to a characteristic intensity value. This relationship enables the determination of an oil-in-water concentration from a measured intensity when the tracer concentration is known, here, 1 mg/L Nile Red in oil.



(a) (b)

Figure 12. (**a**) Fluorescence intensity as function of O/W concentration, the blue data points indicate the measured fluorescence intensity. (**b**) Calibration curve extended to 0–15,000 ppm with PTJ HPO sample results: fluorescence of density-based estimates at 10,000 ppm for selected operating points (red triangles) and corresponding fluorescence-based concentrations (blue markers).

A linear regression equation was fitted to the calibration data:

$$I = m \cdot c_{\mathrm{o/w}}\,[\mathrm{ppm}] + k \tag{7}$$

where I is the fluorescence intensity, and $c_{\mathrm{o/w}}\,[\mathrm{ppm}]$ is the oil-in-water concentration. MATLAB (Version R2023a), was used to determine slope, m, and intercept, k. The resulting values are:

- Intercept $k = 471.96$;
- Slope $m = 1.40$.

This yields

$$I = 1.40 \cdot c_{\mathrm{o/w}}\,[\mathrm{ppm}] + 471.96 \tag{8}$$

with a coefficient of determination $R^2 = 0.9984$, which indicates an excellent linear fit over the investigated concentration range. The intersection point, which is not zero, takes into account the constant background of the imaging system (residual stray light and cuvette-related scattering) at fixed optical settings.

To demonstrate its applicability to PTJ operation, the method was then applied to samples taken at the HPO. For this initial comparison, PTJ operating points were selected for which the density-based evaluation resulted in a residual oil content in the order of 1 vol.%, which corresponds to approximately $c_{\mathrm{o/w}} \approx 10{,}000$ ppm. HPO samples were taken during these operating points. The inlet oil had previously been stained with Nile Red at a concentration of 1 mg/L in the oil phase to ensure a controlled and reproducible fluorometric response.

Figure 12b shows these PTJ samples in relation to the calibration line over an extended concentration range of 0–15,000 ppm. The red triangles show the fluorescence intensity of samples, which showed a concentration of 10,000 ppm in the density-based measurements. The blue markers show the corresponding concentrations determined from the fluorescence intensity using Equation (8). The fluorescence-based concentrations range from 7660 to 12,000 ppm, which indicates a difference of more or less ±20% of the density-based estimation. This representation shows the plausibility and consistency of the method and

confirms that the PTJ outlet samples yield plausible fluorescence signals when processed using the same sample preparation procedure and fixed optical settings as the calibration.

In the next step, the calibration will be validated against TOC measurements with emphasis on the low-ppm range (legal limit 15 ppm) relevant for discharge criteria and operating-window definition. In the present workflow, the fluorescence method complements density-based monitoring by providing rapid ppm-range feedback under reproducible laboratory conditions, enabling efficient screening of operating points and rotor concepts.

5.5. Integration into the PTJ Test Rig and Path Toward In-Line Use

The results show that imaging-based fluorescence can resolve oil-in-water concentrations in the trace range. It, therefore, overcomes the practical ppm-resolution limit of density-based mass-balance monitoring. Under constant optical conditions, a unique relationship between concentration and image signal is obtained. In this study, the mean ROI intensity, I, serves as the quantitative metric.

For application at the PTJ test rig, the method is only quantitative if the optical path is defined and reproducible. This requires a continuous flow cell with fixed geometry, fixed camera position and exposure settings, stable excitation, effective ambient-light shielding, and a repeatable ROI definition. Representative sampling is also required so that the measured fluid reflects the residual oil content at the HPO.

An in-line capable implementation can be realized via a bypass at the HPO. A defined side stream is withdrawn from the HPO discharge line; routed through a short conditioning section, such as a static mixer or a small circulation pump; and then passed through a flow-through cuvette or flow cell placed in the same optical arrangement as the off-line calibration. Camera, lens, filter, illumination and distances remain unchanged. Image acquisition and evaluation can then be executed continuously. The monitored side stream can be returned to the collection tank or disposed of, depending on the test protocol. This approach preserves the applicability of the established calibration procedure while enabling time-resolved monitoring during operating-point sweeps and impeller screening.

A practical limitation of dye-assisted measurements is the need for a separated tracer when non-fluorescent oils are used. At a tracer concentration of 1 mg/L, an oil reservoir of 100 L requires 100 mg (0.1 g) Nile Red. In field-oriented applications, post-dosing is challenging because oil concentration and partitioning conditions are unknown. A controlled tracer concentration in the oil phase cannot be guaranteed without affecting quantification. The present Nile Red-assisted method is, therefore, only for laboratory studies, enabling high-throughput turbomachinery optimization under safe and reproducible conditions. Fortunately, relevant oil pollutions involve substances that are spontaneously fluorescent, so the addition of a tracer is not necessary for practical operation.

6. Conclusions and Future Work

A modified PTJ separation pump combines centrifugal phase separation with pressure buildup and enables compact treatment of oil–water mixtures, where a water-rich stream can be discharged at elevated pressure. The experiments show that the centrifuge reference configuration provides stable separation within a defined operating window, while an impeller with trimmed blades operating primarily in the outer water annulus can substantially increase pressure head at the same rotational speed.

At the same time, the impeller results highlight the design conflict of this apparatus. The impeller improves pressure head, but blade-induced shear and secondary flows promote interfacial entrainment and reduce water purity. Impeller development for PTJ separation pumps, therefore, cannot be guided by hydraulic performance alone. The assess-

ment of ppm-level purity at the HPO must be executed in parallel to define a permissible operating range for each geometry.

To enable iterative optimization with short test cycles, an imaging-based fluorescence oil-in-water concentration measurement method was implemented as a rapid laboratory tool. It bridges the gap between fast but inaccurate density monitoring and accurate but slow TOC analysis. Using sunflower oil dyed with Nile Red at a defined tracer concentration, a robust calibration was obtained with $R^2 = 0.9984$ for the range 5–500 ppm. The first PTJ outlet samples fall within the expected signal range when processed with the same workflow, which supports feasibility for systematic operating-point mapping and impeller screening. At this stage, the method is intended primarily for rapid comparative assessment and operation-window definition.

Future work will proceed along three lines. First, the fluorescence method will be validated against TOC in the lowest ppm range to quantify detection limits and uncertainty under realistic sampling conditions. Second, the imaging setup will be transferred to a bypass-based flow cell to enable time-resolved measurements at the test rig under fixed optical conditions. Third, additional rotor and impeller variants will be evaluated considering both pressure head and ppm-level residual oil at the HPO. The design space will include concepts that reduce interfacial shear, such as casing-side vanes or the Pitot shape acting on the water annulus.

In parallel, CFD will be explored as a supporting tool for systematic geometry studies. The PTJ flow exhibits multiple regimes along the rotor, ranging from dispersed emulsions in the inlet and blade-affected regions to a more segregated structure with a coherent oil core and an interface near the outlets. This multi-regime behavior implies that a single multiphase model is unlikely to capture all relevant flow states with equal fidelity along the rotor. A pragmatic strategy is to use an Euler–Euler approach in regions dominated by dispersed droplets to screen geometry-induced dispersion, losses and mixing trends. Interface-resolving simulations such as VOF can then be applied selectively in the separation region to analyze interface position, stability and entrainment pathways near the HPO.

The present work deliberately relies on experiments as the primary optimization drivers. The main target metric, ppm-level residual oil at the HPO, cannot be predicted with the required reliability at practical computational cost because it depends on subgrid models, droplet breakup, and coalescence and interface contamination mechanisms. CFD is, therefore, suitable for providing qualitative and semi-quantitative guidance, for example, by identifying mixing hot spots, secondary-flow structures and loss mechanisms and by supporting the comparative screening of rotor concepts under controlled boundary conditions. At the same time, the modular additively manufactured platform enables fast and cost-efficient experimental iteration. Alternative concepts, such as straight vanes, casing-side elements and simplified blade geometries, in addition to curved blades, can be printed and validated in back-to-back tests.

Author Contributions: Conceptualization, J.D. and X.Z.; methodology, J.D. and X.Z.; formal analysis, J.D. and X.Z.; investigation, J.D. and X.Z.; data curation, X.Z.; writing—original draft preparation, J.D. and X.Z.; writing—review and editing, K.Z. and D.T.; visualization, J.D.; supervision, K.Z. and D.T.; project administration, J.D.; funding acquisition, J.D. All authors have read and agreed to the published version of the manuscript.

Funding: This project was funded by the DBU under grant number 38123/01-23.

Data Availability Statement: The research data can be provided upon request.

Acknowledgments: We would like to thank the UFZ Leipzig, in particular Jonas Köhne, Katrin Mackenzie and Lucie Moeller, for their active support with the sample analysis.

Conflicts of Interest: The authors declare no conflict of interest.

Abbreviations

The following abbreviations are used in this manuscript:

CF	Coriolis mass flowmeter
CMOS	Complementary metal-oxide-semiconductor
HPO	High-pressure outlet
LPO	Low-pressure outlet
NR	Nile Red
o/w	Oil–water, oil-in-water
ppm	Parts per million (=mg/L for the process considered)
PTJ	Pitot-tube jet (pump)
ROI	Region of interest
TOC	Total organic carbon
c	Oil concentration [mg/L or ppm]
FS	Flow split ratio [−]
c	Chord length [m]
g	Gravitational acceleration [m s^{-2}]
H_{HPO}	Pressure head [m]
I	Intensity
$\dot{m}$	Mass flow rate [kg s^{-1}]
d	Droplet diameter [m]
D	Diameter [mm]
e	Blade thickness [mm]
p	Static pressure [Pa]
n	Rotational speed [min^{-1}]
m	Gradient [−]
k	Intersection [−]
r	Radius [m]
Re	Reynolds number [−]
T	Temperature [°C]
v_{term}	Stokes terminal velocity [m s^{-1}]
α	Oil fraction [−]
β	Blade angle [deg]
κ	Blade curvature radius [mm]
μ	Dynamic viscosity [Pa s]
ρ	Density [kg m^{-3}]

References

1. Sousa, A.M.; Pereira, M.J.; Matos, H.A. Oil-in-water and water-in-oil emulsions formation and de-mulsification. *J. Pet. Sci. Eng.* **2022**, *210*, 110041. [CrossRef]
2. Hu, C.; Herz, C.; Hartman, R.L. Microfluidic dispersion of mineral oil–seawater multiphase flows in the presence of dialkyl sulfonates, polysorbates, and glycols. *Green Process. Synth.* **2013**, *2*, 611–623. [CrossRef]
3. Overton, E.B.; Adhikari, P.L.; Radović, J.R.; Passow, U. Fates of petroleum during the Deepwater Horizon oil spill: A chemistry perspective. *Front. Mar. Sci.* **2022**, *9*, 928576. [CrossRef]
4. Singh, B.J.; Chakraborty, A.; Sehgal, R. A systematic review of industrial wastewater management: Evaluating challenges and enablers. *J. Environ. Manag.* **2023**, *348*, 119230. [CrossRef] [PubMed]
5. Al-Majed, A.A.; Adebayo, A.R.; Hossain, M.E. A sustainable approach to controlling oil spills. *J. Environ. Manag.* **2012**, *113*, 213–227. [CrossRef] [PubMed]
6. Peterson, C.H.; Rice, S.D.; Short, J.W.; Esler, D.; Bodkin, J.L.; Ballachey, B.E.; Irons, D.B. Long-term ecosystem response to the Exxon Valdez oil spill. *Science* **2003**, *302*, 2082–2086. [CrossRef] [PubMed]

7. International Maritime Organization (IMO). MARPOL 1973—Final Act and Convention. Available online: https://wwwcdn.imo.org/localresources/en/KnowledgeCentre/ConferencesMeetings/Documents/MARPOL%201973%20-%20Final%20Act%20and%20Convention.pdf (accessed on 9 February 2026).
8. Kwon, G.; Kota, A.K.; Li, Y.; Sohani, A.; Mabry, J.M.; Tuteja, A. On-demand separation of oil–water mixtures. *Adv. Mater.* **2012**, *24*, 3666–3671. [CrossRef] [PubMed]
9. Yavuz-Düzgün, M.; Kırtıl, E.; Çıkrıkçı-Erünsal, S.; Seçmeler, Ö. Flotation and sedimentation. In *Mechanical Separation Processes in the Food Industry*; Elsevier: Amsterdam, The Netherlands, 2025; pp. 9–60.
10. Jayarathna, M.D.; Rajapaksha, A.U.; Samarasekara, S.; Vithanage, M. Oil Spill Response: Existing Technologies, Prospects and Perspectives. *CleanMat* **2024**, *1*, 78–96. [CrossRef]
11. Muvel, H.; Jindal, M.K.; Tewari, P.K.; Anand, V. Minimizing oil pollution: A review of current status and its treatment options. *RSC Sustain.* **2025**, *3*, 3681–3723. [CrossRef]
12. Semenov, E.V.; Slavyanskiy, A.A.; Mitroshina, D.P. Numerical Analysis of Emulsion Separation Processes in a Continuous Centrifuge. *Chem. Pet. Eng.* **2021**, *57*, 113–121. [CrossRef]
13. Lekomtsev, A.V.; Mordvinov, V.A.; Ilyushin, P.Y.; Bakaneev, V.S.; Kornilov, K.V. Centrifugal Separation in the Treatment of Produced Water for its Subsequent Injection into a Reservoir. *Chem. Pet. Eng.* **2021**, *56*, 979–987. [CrossRef]
14. Meyer, J.; Thévenin, D. Using Centrifugal Forces in a Pitot-Tube Jet-Pump for Cleaning and Pumping Oil-Water Mixtures in a Continuous Loop: An Experimental Study of Separation Efficiency. In Proceedings of the 9th International Conference on Multiphase Flow (ICMF 2016), Firenze, Italy, 22–27 May 2016.
15. Meyer, J. Optimierung Einer Pitot-Pumpe und Deren Adaption zur Öl-Wasser-Trennung. Ph.D. Thesis, Otto von Guericke University Magdeburg, Magdeburg, Germany, 2019.
16. Meyer, J.; Daróczy, L.; Thévenin, D. Shape optimization of the pick-up tube in a Pitot-tube jet pump. *J. Fluids Eng.* **2017**, *139*, 021103. [CrossRef]
17. von Deylen, J.; Köpplin, J.; Thévenin, D. Development and Validation of a Design Tool for an Improved Pitot-Tube Jet-Pump Allowing Continuous Fluid-Fluid Separation. *J. Fluids Eng.* **2022**, *144*, 071401. [CrossRef]
18. NIST Standard Reference Database 69. Thermophysical Properties of Fluid Systems: Isobaric Properties for Water. National Institute of Standards and Technology. 2008. Available online: https://webbook.nist.gov/chemistry/fluid/ (accessed on 9 February 2026).
19. Federation of German Heating Industry (BDH). *Fuel Heating Oil EL: Information Sheet No. 50*; Federation of German Heating Industry (BDH): Cologne, Germany, 2021.
20. Park, S.H.; Youn, I.M.; Lim, Y.; Lee, C.S. Influence of the mixture of gasoline and diesel fuels on droplet atomization, combustion, and exhaust emission characteristics in a compression ignition engine. *Fuel Process. Technol.* **2013**, *106*, 392–401. [CrossRef]
21. Ichu, C.B.; Nwakanma, H.O. Comparative study of the physicochemical characterization and quality of edible vegetable oils. *Int. J. Res. Inf. Sci. Appl. Technol.* **2019**, *3*, 1–9. [CrossRef]
22. Dafis, J.; Zhang, X.; Zähringer, K. Mobile Separation of Complex Oil-Water Mixtures with an Adapted Pitot Pump. In Proceedings of the 19th International Conference on Fluid Flow Technologies (CMFF'25), Budapest, Hungary, 26–29 August 2025.
23. Dafis, J.; Hagemeier, T.; Müller, D.; Zähringer, K. A new fluorescence imaging method to evaluate different oil types and their concentrations in water. *Chem. Eng. Technol.* **2025**, *48*, e70128. [CrossRef]
24. Köpplin, J.; Bednarz, L.; Hagemeier, T.; Thévenin, D. Fluorescence imaging methodology for oil-in-water concentration measurements. *Chem. Eng. Technol.* **2021**, *44*, 1343–1349. [CrossRef]

Disclaimer/Publisher's Note: The statements, opinions and data contained in all publications are solely those of the individual author(s) and contributor(s) and not of MDPI and/or the editor(s). MDPI and/or the editor(s) disclaim responsibility for any injury to people or property resulting from any ideas, methods, instructions or products referred to in the content.